ACS APPLIED MATERIALS & INTERFACES

Research Article

www.acsami.org

Synergetic Gating of Metal-Latching Ligands and Metal-Chelating Proteins for Mesoporous Silica Nanovehicles to Enhance Delivery Efficiency

Shanshan Wu, Qingqing Deng, Xuan Huang, and Xuezhong Du*

Key Laboratory of Mesoscopic Chemistry (Ministry of Education), State Key Laboratory of Coordination Chemistry, School of Chemistry and Chemical Engineering, Nanjing University, Nanjing 210093, People's Republic of China

Supporting Information

ABSTRACT: Stimuli-responsive drug delivery systems are highly desirable for improved therapeutic efficacy and minimized adverse effects of drugs. Mesoporous silica nanoparticles (MSNs) functionalized with pentadentate ligands, *N*-(3-trimethoxysilylpropyl)ethylenediamine triacetate (TSP-DATA), in the presence of metal ions with and without myoglobin (Mb)-containing surface-accessible histidine residues, were constructed for pH-triggered controlled release. The DATA ligands immobilized on the MSN pore outlets could encapsulate cargo within the pores by metal latching across pore openings, and release efficiency increased with the increase of surface density of the DATA ligands. The release efficiencies for the metal-chelating protein nanogates, through multiple-site binding of Mb with the metal-chelating ligands, were higher than those for the metal-latching ligand nanogates but were almost independent of surface density of the ligands investigated. Both the metal-latching ligands and the metal-chelating proteins played a synergetic role in gating MSNs for high-loading drug delivery and stimuli-responsive controlled release. The constructed Mb−Cu^{2+}-gated MSN delivery system has promising applications in targeted drug therapy of tumors.

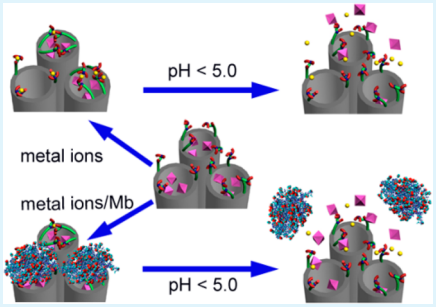

KEYWORDS: *controlled release, drug delivery, histidine residue, metal-chelating ligand, mesoporous silica nanoparticle, protein*

INTRODUCTION

There has been an ever increasing interest in developing stimuli-responsive drug delivery systems to improve therapeutic efficacy and minimize adverse effects of drugs.[1] In comparison with polymeric nanoparticles, micelles, and liposomes, mesoporous silica nanoparticles (MSNs) have emerged as promising drug delivery systems because of high surface area, large pore volume, tunable pore size, good biocompatibility, and easy functionalization.[2−8] To date, inorganic nanoparticles,[9] organic molecules,[10−13] and biomolecules[14] have been used as MSN gatekeepers to show well-controlled release performances. The controlled release can be regulated by various stimuli, such as pH,[10,14] competitive binding,[9] redox,[10,14] light,[11] heat,[12] and enzyme.[13] Biomacromolecules as gatekeepers provide inherent biocompatibility and better cellular uptake and are highly desirable under disease-related environments for practical applications; however, the direct use of biomolecules as gatekeepers is still in its infancy. In comparison to DNA and tailor-made oligonucleotides for complementary hybridization as gatekeepers,[15−21] few examples of proteins as gatekeepers have been so far reported despite a great variety of proteins. One example was the redox-responsive collagen-gated MSN system via covalent linkages containing disulfide bonds,[22] whereas this gating was independent of specificity of proteins. A strategy based on the ligand−protein interactions is used for construction of stimuli-responsive protein-gated MSN systems functionalized with specific ligands. The biotin−avidin complex with a binding constant of 10^{13}−10^{15} M^{-1} is the strongest noncovalent interaction found in nature; however, avidin as a nanogate cannot easily be opened in a mild manner for controlled release of drugs in biological applications because of its strong affinity for the biotinylated MSN surface.[23] One successful example was based on the antibody−hapten interaction with a good affinity to construct the antibody-gated MSN system functionalized with hapten for controlled release by competitive binding of antigen.[24] Multivalent carbohydrate−protein interactions improve the interaction strength and specificity in comparison to weak monovalent interactions.[25−28] Recently, a delivery system of concanavalin A-gated MSNs functionalized with mannose ligands was constructed for pH- and glucose-responsive controlled release based on the multivalent carbohydrate−protein interactions.[29]

The specific binding of proteins, with exposed histidine (His) residues, to the surfaces derived with Cu^{2+}-chelating iminodiacetate (IDA)[30−32] or Ni^{2+}-chelating nitrilotriacetate (NTA)[33−35] is commonly used for immobilization and purification of proteins. IDA can bind Cu^{2+} strongly with a binding constant of about 10^{10} M^{-1},[30] and the IDA−Cu^{2+} complex in turn binds a single His residue with a moderate affinity ($10^{3.5}$ M^{-1}).[30] It has been shown that multiple-site

Received: June 4, 2014
Accepted: August 12, 2014
Published: August 12, 2014

binding of the proteins containing two surface accessible His residues to the surfaces densely derived with the IDA–Cu^{2+} complexes results in apparent protein binding constants greater than 10^6 M^{-1}.[30,36]

Recently, Qu et al. constructed a delivery system of His-tagged fluorescent protein-gated magnetic MSNs functionalized with Ni^{2+}-chelating NTA ligands for controlled release by competitive binding of His (50 mM).[37] Herein, surface His-rich native proteins, without additional His tag, were used for the construction of protein-gated MSN systems functionalized with metal-chelating ligands, *N*-(3-trimethoxysilylpropyl)-ethylenediamine triacetate (TSP-DATA), for pH-responsive controlled release (Scheme 1). Myoglobin (Mb) contains 11

Scheme 1. Illustration of Synergetic Gating of Metal Latching and Metal-Chelating Myoglobin (Mb) for MSNs Functionalized with the Pentadentate Ligands of Ethylenediamine Triacetate (DATA) and pH-Responsive Controlled Release

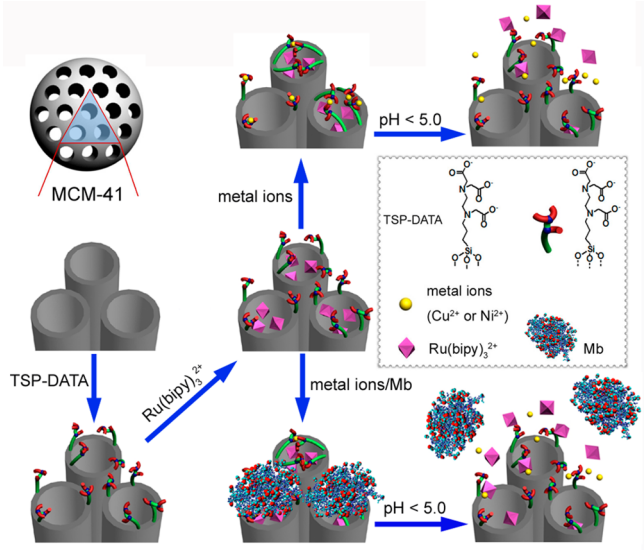

His residues, five of which are on the outer exposed surface in the native state[31,32,38] available for multiple-site binding. DATA is a pentadentate ligand and contains an IDA unit or an NTA-like unit. In the presence of transition metal ions, there are a few types of probable metal chelating. The 1:1 metal–DATA complexes on the MSN surface still had free coordination sites available for binding of surface His-rich proteins, and the 1:2 metal–DATA complexes could block the MSN pores when the complexes formed over pore openings even in the absence of proteins. Both metal-latching ligands and metal-chelating proteins, closely related to metal coordination, played a synergetic role in gating MSNs for high-loading drug delivery and stimuli-responsive controlled release.

EXPERIMENTAL SECTION

Materials. Tetraethylorthosilicate (TEOS, 99%) and Mb (pI 7.3, 17 kDa, 2.5 × 4.4 × 4.4 nm) from equine skeletal muscle were purchased from Sigma-Aldrich. Cetyltrimethylammonium bromide (CTAB) and sodium hydroxide (NaOH) were purchased from Shanghai Reagent Co., Ltd. (China). Tris(2,2′-bipyridyl)ruthenium-(II) chloride hexahydrate ($Ru(bipy)_3^{2+}$) were purchased from Aladdin. *N*-(3-Trimethoxysilylpropyl)ethylenediamine triacetate trisodium salt (TSP-DATA, 45%) in water was purchased from Fluorochem Ltd. Unit. Copper chloride dihydrate and nickel chloride hexahydrate were purchased from Nanjing Chemical Reagent Co., Ltd. Doxorubicin hydrochloride (DOX) was purchased from Meilun Biology Co. (Dalian, China). The buffer solution (10 mM, pH 7.2) was prepared from 4-(2-hydroxyerhyl)piperazine-1-ethanesulfonic acid (HEPES), and the pH was adjusted with HCl and NaOH. All of the chemicals used were of analytical grade, and water used was double-distilled.

Synthesis of MCM-41. MCM-41 was synthesized according to the base-catalyzed sol–gel method. CTAB surfactants (0.5 g) were dissolved in 240 mL of distilled water, and then 1.75 mL of aqueous NaOH solution (2.0 M) was added. After the mixture was heated to 80 °C, TEOS (2.5 mL) was added dropwise over 10 min. The reaction was allowed to proceed under stirring for 2 h. The white precipitates were collected by filtration, then thoroughly washed with methanol and water, and finally dried under vacuum. The CTAB surfactants were removed by heating 1.0 g of the as-synthesized nanoparticles in 100 mL of methanol and 6.0 mL of concentrated HCl solution under reflux for 24 h. The MCM-41 nanoparticles were centrifuged, washed copiously with methanol, and dried under vacuum.

Preparation of DATA-Modified MSNs. MSNs (100 mg) were suspended in 30 mL of methanol solution containing different amounts of TSP-DATA (10, 25, or 125 μL) and stirred at 80 °C under nitrogen for 12 h. The modified products were referred to as MT. The MT series with different surface densities of the DATA ligands were in turn denoted as MT1, MT2, and MT3. The accurate surface densities of functionalized DATA were determined by thermogravimetric analysis. The MT series was collected, washed with methanol, and dried under vacuum.

Cargo Loading, Metal (Cu^{2+} or Ni^{2+}) Chelating, and Protein Capping. MT (0.02 g) was dispersed in 3 mL of the HEPES buffer solution (10 mM, pH 7.2) containing $Ru(bipy)_3^{2+}$ (1 mM) under stirring for 24 h at room temperature for cargo loading. 6.7 mg of Mb and 40 μL of aqueous solution of Cu^{2+} or Ni^{2+} (10 mM) were then added, and the mixture was stirred for 12 h to allow for the interactions of the His residues on the Mb surface with the functionalized DATA ligands via Cu^{2+} or Ni^{2+} coordination to cap the MSN pore entrances. The $Ru(bipy)_3^{2+}$-loaded, Mb-metal-gated MT systems were collected by filtration and washed thoroughly with the HEPES buffer solution (pH 7.2) until no dye leakage was visible to the naked eyes. The $Ru(bipy)_3^{2+}$-loaded, metal-latched MT systems followed the similar procedure in the absence of Mb for comparison. The loading capacities of $Ru(bipy)_3^{2+}$ for various MSN materials were calculated from the difference between the initially added (total) and unloaded (washed) amounts of cargo.

Cargo Release. To investigate premature release of the delivery systems, both the $Ru(bipy)_3^{2+}$-loaded, metal-latched MT series and the $Ru(bipy)_3^{2+}$-loaded, Mb-metal-gated MT series were dispersed in 5 mL of the HEPES buffer solution (pH 7.2) in a dialysis bag (molecular weight cutoff of 8000), and then the sealed dialysis bag was submerged in 15 mL of the HEPES buffer solution (pH 7.2). To investigate the stimuli-responsive controlled release profiles of the cargo, the pH of the HEPES buffer solution was changed from 7.4 to 5.0 and, additionally, to 3.0. The amounts of released $Ru(bipy)_3^{2+}$ in the buffer solutions were monitored using UV–vis spectroscopy with the absorption maximum of $Ru(bipy)_3^{2+}$ at 453 nm.

DOX Loading and Release. MT2 (0.02 g) was dispersed in 3 mL of the HEPES buffer solution (10 mM, pH 7.2) containing DOX (0.5 mM) under stirring for 24 h for DOX loading. Mb (6.7 mg) and an aqueous solution of Cu^{2+} (10 mM, 40 μL) were then added, and the mixture was stirred for 12 h. The DOX-loaded, Mb–Cu^{2+}-gated MT2 was collected by filtration and washed thoroughly with the HEPES buffer solution (pH 7.2) until no dye leakage was visible to the naked eyes. To investigate the pH-responsive DOX release profiles, the DOX-loaded, Mb–Cu^{2+}-gated MT2 system was dispersed in 5 mL of the HEPES buffer solution at different pH values in a dialysis bag, and the sealed dialysis bag was then submerged in 10 mL of the HEPES buffer solution at the corresponding pH. The HEPES buffer solutions containing the released DOX were collected at different time intervals for spectral analysis and replaced with an equal volume of fresh HEPES buffer. The amounts of released DOX in the buffer solutions

were monitored using fluorescence spectroscopy with the emission maximum of DOX at 556 nm.

Cytotoxicity Assay. The DOX-loaded, Mb−Cu^{2+}-gated MT2 nanoparticles were collected by centrifugation and stored in a freeze dryer at −10 °C. To test the cytotoxicity of Mb−Cu^{2+}-gated MT2, A549 cells were seeded in a 96-well plate at a density of 8000 cells/well for 24 h, and then the cells were incubated with Mb−Cu^{2+}-gated MT2 at various concentrations (2.5, 5, 10, 20, 40, 80, 160, and 320 μg/mL) without and with loading of DOX. After 48 h of incubation, the cells were continuously incubated in the wells containing 5 mg/mL of 3-(4,5-dimethylthiazol-2-yl)-2,5-diphenyltetrazolium bromide (MTT) for 4 h. Afterward, the crystallized formazan violet were redissolved in 150 μL of dimethyl sulfoxide at 37 °C. The absorbance at 490 nm was measured by a multidetection microplate reader.

Instruments and Measurements. The scanning electron microscope (SEM) and transmission electron microscope (TEM) images of the MSN materials were acquired on a Hitachi S-4800 microscope and on a JEM-2100 microscope, respectively. Powder X-ray diffraction (XRD) measurements were performed on a Thermo ARL SCINTAG X'TRA diffractometer using a Cu Kα radiation (λ = 0.154 05 nm). The surface areas, cumulative pore volumes, and pore size distributions of the MSN materials were determined from nitrogen adsorption−desorption isotherms measured on an ASAP2020 porosimeter at 77 K. Thermogravimetric analyses were carried out on a TGA/SDT2960 thermogravimetric analyzer, using an oxidant atmosphere (air, 80 mL/min) with a heating rate of 10 °C per minute from room temperature to 1000 °C. Hydrodynamic size distributions of the MSN materials were determined by dynamic light scattering using a 90Plus particle size analyzer (Brookhaven Instruments Co.), and zeta potentials were measured using a zeta potential analyzer (ZetaPALS, Brookhaven Instruments Co.). Fourier transform infrared (FTIR) spectra were recorded on a VECTORTM 22 spectrometer, UV−vis spectra were collected on a UV-Lambda35 spectrometer, and fluorescence spectra were measured on a Shimadzu RF-5301PC spectrofluorophotometer. MTT assays were carried out on a BioTek-Instruments.

RESULTS AND DISCUSSION

Construction of Mb−Cu^{2+}-Gated MSN Vehicles. MCM-41 was synthesized using a base-catalyzed sol−gel method. The SEM image shows that MSNs were uniform and spherical with an average diameter of 125 nm, and the TEM image shows that MSNs had hexagonal-packed mesostructures with parallel cylindrical channels (Supporting Information, Figure S1). MCM-41 was functionalized with DATA, referred to as MT, and the DATA-modified MSNs with different surface densities of the ligands were denoted as MT1, MT2, and MT3. The surface densities of the DATA ligands were determined by thermogravimetric analysis to be 0.20, 0.32, and 0.51 mmol/g for M1, M2, and M3, respectively (Supporting Information, Figure S2). After the MT series were capped with Mb (without cargo loading) in the presence of Cu^{2+} ions, the capping amounts of Mb for the MT1, MT2, and MT3 systems were also determined by thermogravimetric analysis to be 0.056, 0.079, and 0.123 g/g, respectively (Supporting Information, Figure S2). The SEM and TEM images of the MT series did not show significant differences from those of MCM-41, whereas the mesoporous structures of the Mb−Cu^{2+}-gated MT series without cargo loading became unclear with the increase of surface density of the DATA ligands, particularly for Mb−Cu^{2+}-gated MT3 (Supporting Information, Figure S3), probably owing to the capping of Mb in a large amount.

FTIR spectroscopy was used to characterize the functionalization of DATA and capping of Mb. Obvious spectral features were observed for MT3 with two bands at 1600 and 1406 cm^{-1} (Supporting Information, Figure S4), assigned to the antisymmetric and symmetric stretching vibrations of carboxylate groups, respectively, which means that MCM-41 was functionalized with DATA. After Mb binding in the presence of Cu^{2+} ions, two strong bands at 1655 and 1540 cm^{-1} were obviously observed (Supporting Information, Figure S5), due to the amide I and amide II bands of the protein, respectively, and their intensities (corresponding to amounts of bound proteins) increased with the increase of surface density of the DATA ligands. The FTIR results of Mb capping for the MT series were consistent with the data of thermogravimetric analyses.

The nitrogen adsorption−desorption isotherms of MCM-41 showed typical curves of type IV with a surface area of 1020 m^2/g and an average pore size of 2.62 nm (Supporting Information, Figure S6 and Table S1). The surface area and pore size of the MT series decreased with the increase of surface density of the DATA ligands. In the case of MT2, the surface area was decreased to 782 m^2/g, and after loading of the cargo $Ru(bipy)_3^{2+}$, Cu^{2+}-latched MT2 had a surface area of 243 m^2/g with the filling of most of the pores. For the cargo-loaded, Mb−Cu^{2+}-gated MT2 system, the surface area was further reduced to 92 m^2/g, and the pores were filled and capped (Supporting Information, Figure S7 and Table S1). The loading capacity of $Ru(bipy)_3^{2+}$ were determined using UV−vis spectroscopy to be 0.073, 0.084, 0.087, 0.094, 0.102, and 0.101 mmol/g for Cu^{2+}-latched MT1, Cu^{2+}-latched MT2, Cu^{2+}-latched MT3, Mb−Cu^{2+}-gated MT1, Mb−Cu^{2+}-gated MT2, and Mb−Cu^{2+}-gated MT3, respectively (Supporting Information, Figure S8). For the Cu^{2+}-latched MT systems, the cargo loading capacity increased with the increase of the surface density of the DATA ligands, moreover the protein capping improved the cargo loading capacities.

The small-angle powder X-ray diffraction (XRD) patterns of MCM-41 displayed three reflection peaks at (100), (110), and (200) planes (Supporting Information, Figure S9), typical of a hexagonal mesoporous structure. From the XRD and porosimetry, the thickness of silica wall (1.96 nm) could be calculated from the difference between the cell parameter $a_0 = 2 \times d_{100}/\sqrt{3}$ = 4.58 nm (d_{100} is the d(100) spacing) and the Barrett−Joyner−Halenda (BJH) pore diameter (2.62 nm). The MT series also showed similar XRD patterns to MCM-41, which indicates that the modified DATA ligands did not have an influence on the mesoporous structure of the silica matrix. However, none of the three peaks could be detectable after loading with $Ru(bipy)_3^{2+}$ and capping with Mb in the presence of Cu^{2+} ions, owing to an effect from the filled pores.

The zeta potentials of MCM-41, MT2, and Mb−Cu^{2+}-gated MT2 in the HEPES buffer solutions (10 mM, pH 7.2) were −20.5, −41.0, and −19.0 mV, respectively (Supporting Information, Figure S10), and the average hydrodynamic diameters of the corresponding nanoparticles were 109, 117, and 138 nm, respectively (Supporting Information, Figure S11). These results indicate that Mb−Cu^{2+}-gated MT2 was negative-charged and could be well-dispersed in aqueous solutions.

Synergetic Gating and Controlled Release. UV−vis spectroscopy was first used to check for premature release of $Ru(bipy)_3^{2+}$ from the Cu^{2+}-latched MT and Mb−Cu^{2+}-gated MT series, with the absorption maximum of $Ru(bipy)_3^{2+}$ at 453 nm (Supporting Information, Figures S12−S14). As shown in Figure 1, both the Cu^{2+}-latched MT and Mb−Cu^{2+}-gated MT systems in the HEPES buffer solutions (pH 7.2) showed a good blocking performance, especially for the Mb−Cu^{2+}-gated MT2 and Mb−Cu^{2+}-gated MT3 systems with a minimal premature

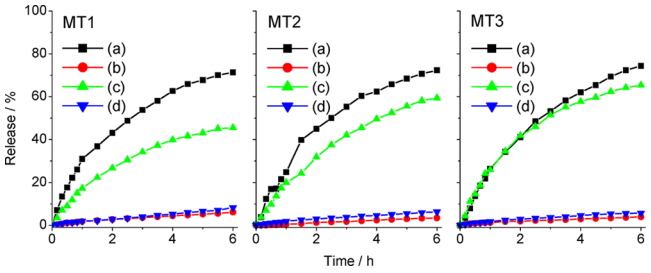

Figure 1. pH-triggered release profiles of $Ru(bipy)_3^{2+}$ from the MT1, MT2, and MT3 systems in the HEPES buffer solutions: (a) Mb−Cu^{2+}-gated MT series at pH 3.0, (b) Mb−Cu^{2+}-gated MT series at pH 7.2, (c) Cu^{2+}-latched MT series at pH 3.0, (d) Cu^{2+}-latched MT series at pH 7.2. The release efficiencies of various systems were calculated with their respective cargo loading capacities.

release up to 6 h. Recently, Zink et al. reported pH-responsive IDA-functionalized MSN delivery systems with metal-latched nanogates.[39] It is shown that only metal chelating could well block the MSN pores. MSNs are comprised of two-dimensional hexagonal porous structures with cylindrical pores running from one end of the sphere to the other. This unique feature renders the capability of no leaking even in the case of incomplete capping; that is, absence of control of a pore results only in the loss of the cargo of that pore.[1] Upon decreasing the pH of the buffer solutions to 3.0, the release efficiencies of the cargo from the Cu^{2+}-latched MT and Mb−Cu^{2+}-gated MT systems significantly increased, because of the removal of Cu^{2+} ions and Cu^{2+} ions/Mb from the immobilized DATA ligands. The corresponding release profiles, where the release efficiencies of various systems were calculated with a maximum loading capacity of 0.102 mmol/g as a reference, are presented in Supporting Information, Figure S15 for comparison.

To clarify the metal-chelating effect, Mb−Cu^{2+}-gated MT2 and corresponding counterpart (prepared in the absence of Cu^{2+} ions) were compared (Figure 2 and Supporting Information, Figure S16). The counterpart showed slight release of the cargo after the trigger of pH 3.0, which resulted from the desorption of a small amount of $Ru(bipy)_3^{2+}$ adsorbed on the MT2 surface (a zeta potential of −41.0 mV) due to the

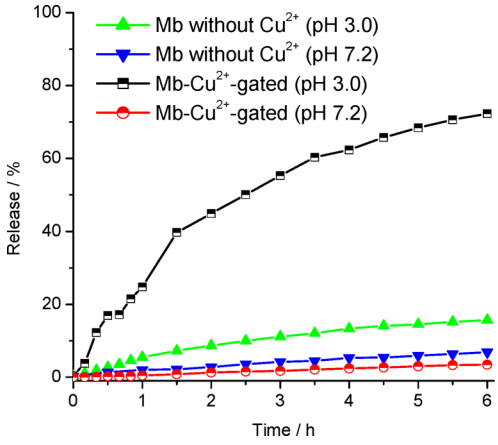

Figure 2. Comparison of pH-triggered release profiles of $Ru(bipy)_3^{2+}$ from the MT2 systems without Cu^{2+} in the presence of Mb in the HEPES buffer solutions with the Mb−Cu^{2+}-gated MT2 systems at pH 7.2 and 3.0. The release efficiencies of different systems were calculated with the maximum cargo loading capacity of Mb−Cu^{2+}-gated MT2 system.

electrostatic interaction upon reduction of pH. In the absence of Cu^{2+} ions, the DATA ligands could not be latched across pore openings; Mb could not be chelated for capping the MSN pores. The cargo was washed off even if loaded, so that no cargo could be released except for a small amount of adsorbed cargo. The FTIR spectrum of the counterpart did not show amide I or amide II bands of the proteins, which indicates that the proteins did not suffer a nonspecific adsorption on the MT2 surface in the absence of Cu^{2+} ion (Supporting Information, Figure S5e). The comparative study demonstrates that metal chelating could encapsulate cargo within the MSN pores and regulate release of cargo from the pores and that the protein capping was realized by specific binding of the proteins to the metal-chelating ligands. These results indicate that metal-latching ligands and metal-chelating proteins as nanogates played an important role in encapsulating cargo and controlling cargo release.

For the Cu^{2+}-latched MT systems, the loading capacity and release efficiency of the cargo increased with the increase of surface density of the DATA ligands. The possibility of the development of the 1:2 metal−DATA complexes across MSN pore openings increased with the increase of the surface density of the DATA ligands. The loading capacities and release efficiencies of the cargo for the Mb−Cu^{2+}-gated MT systems were higher than those for the corresponding Cu^{2+}-latched MT systems, but the release efficiencies of the Mb−Cu^{2+}-gated MT systems were nearly comparable and almost independent of surface density of the ligands investigated. Taking into account the dimensions of Mb (2.5 × 4.4 × 4.4 nm), the size of the pores (2.62 nm), and the thickness of silica walls (1.96 nm), the dimensions of Mb could well match with the pore size and wall thickness, and the pores could be effectively blocked with the capping of Mb. Obviously, the metal-chelating proteins improved the loading capacities and release efficiencies of the cargo. Both metal-latching ligands and metal-chelating proteins were closely related to metal coordination and had a synergetic effect of nanogates. Clearly, both metal-latching ligands and metal-chelating proteins played a synergetic role in gating MSNs for high-loading drug delivery and stimuli-responsive controlled release.

With the increase of surface density of the DATA ligands, the number of the MSN pores covered with the metal-latching ligands (1:2 metal−DATA complexes) increased, and the amount of metal-chelating proteins also increased, through multiple-site binding of Mb with available free coordination sites in the 1:1 and 1:2 metal−DATA complexes. If the metal-chelating proteins with multiple-site binding tightly capped the pore openings (unblocked pores), more cargo could be encapsulated within the pores, and the release efficiency of the cargo was accordingly improved. If the metal-chelating proteins covered the pores already blocked with the metal-latching ligands on the pore outlets, this part of the metal-chelating proteins would have no significant contribution to the encapsulation and release of cargo. This is the reason that the release efficiency hardly increased with the increasing amount of bound proteins.

After the release of cargo at pH 3.0, the Mb−Cu^{2+}-gated MT2 system showed the same FTIR spectrum as MT2 with the disappearance of the amide I and amide II bands of the proteins (Supporting Information, Figure S5), which confirmed that the Cu^{2+} ions and Mb were removed from the MT2 surface for release of cargo; the surface area returned from 92 m^2/g to 598 m^2/g, and the pore size was restored to 2.19 nm (Supporting

Information, Figure S7 and Table S1); the XRD reflection peaks reappeared but with reduced intensities (Supporting Information, Figure S9). All of these changes indicate that the two nanogates of metal-latching ligands and metal-chelating proteins of the delivery system opened and the cargo was released under acidic conditions, although there was a small amount of cargo retained in the pores.

Ni^{2+} coordination was also tested for the MT2 systems. The release profiles of the cargo from the Ni^{2+}-latched MT2 and Mb−Ni^{2+}-gated MT2 systems were compared to the Cu^{2+}-latched MT2 and Mb−Cu^{2+}-gated MT2 systems upon decreasing of the pH from 7.2 to 5.0, and additionally to 3.0 (Figure 3 and Supporting Information, Figure S17). The

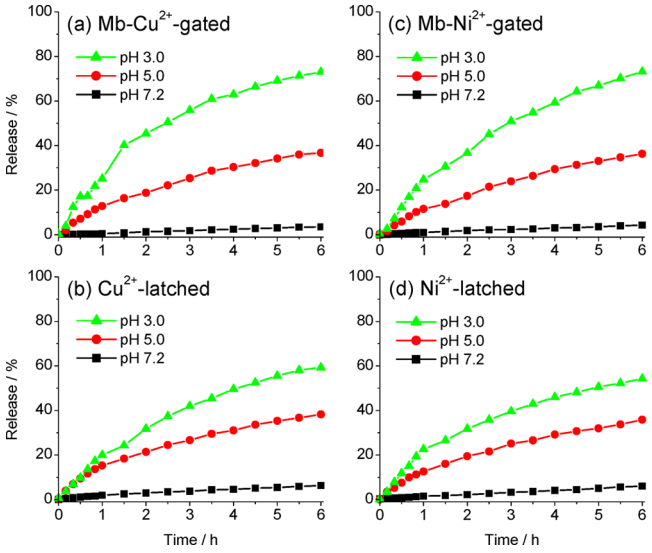

Figure 3. pH-triggered release profiles of $Ru(bipy)_3^{2+}$ from the MT2-related systems in the HEPES buffer solutions: (a) Mb−Cu^{2+}-gated MT2 at pH 7.2, 5.0, and 3.0; (b) Cu^{2+}-latched MT2 at pH 7.2, 5.0, and 3.0; (c) Mb−Ni^{2+}-gated MT2 at pH 7.2, 5.0, and 3.0; (d) Ni^{2+}-latched MT2 at pH 7.2, 5.0, and 3.0.

blocking performances and pH-triggered controlled release of the delivery systems in the case of Ni^{2+} ions were nearly the same as those in the case of Cu^{2+} ions. This is because the pentadentate ligands containing an IDA unit or an NTA-like unit have strong coordination interactions with a variety of transition metal ions.

Drug Release, Cytotoxicity, and Antitumor Efficiency. To investigate potential biological applications of the constructed nanovehicles, the pH-responsive controlled release of the antitumor drug DOX from DOX-loaded, Mb−Cu^{2+}-gated MT2 systems was investigated (Figure 4a). The loading capacity of DOX was determined using fluorescence spectroscopy to be 0.067 mmol/g (Supporting Information, Figure S18). At pH 5.0, significant DOX release was observed in comparison to the case at pH 7.2. Furthermore, the in vitro cytotoxicity and antitumor efficiency of the Mb−Cu^{2+}-gated MT2 systems without and with loading of DOX were evaluated by the MTT assay after 48 h of incubation with A549 cells (Figure 4b). Mb−Cu^{2+}-gated MT2 without drug loading showed a low cytotoxicity after 48 h of incubation; however, Mb−Cu^{2+}-gated MT2 with DOX loading showed antiproliferative activity against A549 cells with a cell viability smaller than 20%. This indicates that the constructed Mb−Cu^{2+}-gated MT delivery system for pH-responsive controlled release has

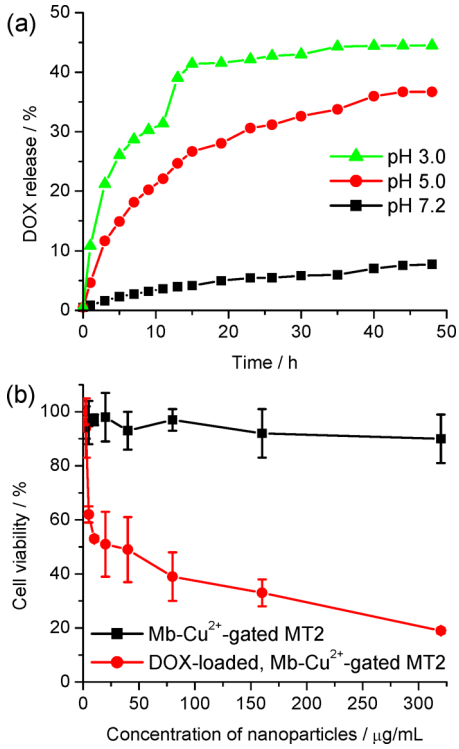

Figure 4. (a) pH-triggered release profiles of DOX from the Mb−Cu^{2+}-gated MT2 systems in the HEPES buffer solutions at different pH. (b) Cell viability of Mb−Cu^{2+}-gated MT2 without and with loading of DOX after 48 h of incubation with A549 cells.

promising applications in site-specific tumor therapy because tumor cells usually have an acidic environment.

CONCLUSIONS

The pH-responsive delivery systems of DATA-functionalized MSNs in the presence of metal ions (Cu^{2+} or Ni^{2+}) with and without Mb capping were constructed. Both metal-latching ligands and metal-chelating proteins played an important role in encapsulating and releasing cargo. The release efficiency for the nanogates of metal-latching ligands across pore openings increased with the increase of surface density of the DATA ligands. The release efficiencies for the metal-chelating protein nanogates, through multiple-site binding of Mb with the metal-chelating ligands, were higher than those for the metal-latching nanogates but were almost independent of surface density of the ligands investigated. Both the metal-latching ligands and the metal-chelating proteins played a synergetic role in gating MSNs for high-loading drug delivery and stimuli-responsive controlled release. The constructed Mb−Cu^{2+}-gated MSN delivery system has promising applications in targeted drug therapy of tumors.

ASSOCIATED CONTENT

Supporting Information

SEM and TEM images, thermogravimetric analyses, FTIR spectra, nitrogen adsorption−desorption isotherms and pore size distributions, UV−vis spectra and working curve, fluorescence spectra and working curve, small-angle XRD, zeta potentials, hydrodynamic diameters, and time-dependent UV−vis spectra of cargo release and pH-responsive release profiles. This material is available free of charge via the Internet at http://pubs.acs.org.

AUTHOR INFORMATION

Corresponding Author

*E-mail: xzdu@nju.edu.cn.

Notes

The authors declare no competing financial interest.

ACKNOWLEDGMENTS

This work was supported by National Natural Science Foundation of China (No. 21273112) and Natural Science Foundation of Jiangsu Province (BK2012719).

REFERENCES

(1) Slowing, I. I.; Vivero-Escoto, J. L.; Wu, C.-W.; Lin, V. S.-Y. Mesoporous Silica Nanoparticles as Controlled Release Drug Delivery and Gene Transfection Carriers. *Adv. Drug Delivery Rev.* **2008**, *60*, 1278−1288.

(2) Coti, K. K.; Belowich, M. E.; Liong, M.; Ambrogio, M. W.; Lau, Y. A.; Khatib, H. A.; Zink, J. I.; Khashab, N. M.; Stoddart, J. F. Mechanised Nanoparticles for Drug Delivery. *Nanoscale* **2009**, *1*, 16−39.

(3) Popat, A.; Hartono, S. B.; Stahr, F.; Liu, J.; Qiao, S. Z.; Lu, G. Q. Mesoporous Silica Nanoparticles for Bioadsorption, Enzyme Immobilisation, and Delivery Carriers. *Nanoscale* **2011**, *3*, 2801−2818.

(4) Yang, Y.-W. Towards Biocompatible Nanovalves Based on Mesoporous Ssilica Nanoparticles. *Med. Chem. Commun.* **2011**, *2*, 1033−1049.

(5) Yang, P.; Gai, S.; Lin, J. Functionalized Mesoporous Silica Materials for Controlled Drug Delivery. *Chem. Soc. Rev.* **2012**, *41*, 3679−3698.

(6) Coll, C.; Bernardos, A.; Martínez-Máñez, R.; Sancenon, F. Gated Silica Mesoporous Supports for Controlled Release and Signaling Applications. *Acc. Chem. Res.* **2013**, *46*, 339−349.

(7) Argyo, C.; Weiss, V.; Bräuchle, C.; Bein, T. Multifunctional Mesoporous Silica Nanoparticles as a Universal Platform for Drug Delivery. *Chem. Mater.* **2014**, *26*, 435−451.

(8) Chen, Y.; Chen, H.; Shi, J. Inorganic Nanoparticle-Based Drug Codelivery Nanosystems to Overcome the Multidrug Resistance of Cancer Cells. *Mol. Pharmaceutics* **2014**, *11*, 2495−2510.

(9) Zhu, C.-L.; Lu, C.-H.; Song, X.-Y.; Yang, H.-H.; Wang, X.-R. Bioresponsive Controlled Release Using Mesoporous Silica Nanoparticles Capped with Aptamer-Based Molecular Gate. *J. Am. Chem. Soc.* **2011**, *133*, 1278−1281.

(10) Wang, C.; Li, Z.; Cao, D.; Zhao, Y.-L.; Gaines, J. W.; Bozdemir, O. A.; Ambrogio, M. W.; Frasconi, M.; Botros, Y. Y.; Zink, J. I.; Stoddart, J. F. Stimulated Release of Size-Selected Cargos in Succession from Mesoporous Silica Nanoparticles. *Angew. Chem., Int. Ed.* **2012**, *51*, 5460−5465.

(11) Guardado-Alvarez, T. M.; Devi, L. S.; Russell, M. M.; Schwartz, B. J.; Zink, J. I. Activation of Snap-Top Capped Mesoporous Silica Nanocontainers Using Two Near-Infrared Photons. *J. Am. Chem. Soc.* **2013**, *135*, 14000−14003.

(12) Aznar, E.; Mondragón, L.; Ros-Lis, J. V.; Sancenón, F.; Marcos, M. D.; Martínez-Máñez, R.; Soto, J.; Pérez-Payá, E.; Amorós, P. Finely Tuned Temperature-Controlled Cargo Release Using Paraffin-Capped Mesoporous Silica Nanoparticles. *Angew. Chem., Int. Ed.* **2011**, *50*, 11172−12275.

(13) Popat, A.; Ross, B. P.; Liu, J.; Jambhrunkar, S.; Kleitz, F.; Qiao, S. Z. Enzyme-Responsive Controlled Release of Covalently Bound Prodrug from Functional Mesoporous Silica Nanospheres. *Angew. Chem., Int. Ed.* **2012**, *51*, 12486−12489.

(14) Xiao, D.; Jia, H.-Z.; Zhang, J.; Liu, C.-W.; Zhuo, R.-X.; Zhang, X.-Z. A Dual-Responsive Mesoporous Silica Nanoparticle for Tumor-Triggered Targeting Drug Delivery. *Small* **2014**, *10*, 591−598.

(15) Torney, F.; Trewyn, B. G.; Lin, V. S.-Y.; Wang, K. Mesoporous Silica Nanoparticles Deliver DNA and Chemicals into Plants. *Nat. Nanotechnol.* **2007**, *2*, 295−300.

(16) Climent, E.; Martínez-Máñez, R.; Sancenón, F.; Marcos, M. D.; Soto, J.; Maquieira, A.; Amorós, P. Controlled Delivery Using Oligonucleotide-Capped Mesoporous Silica Nanoparticles. *Angew. Chem., Int. Ed.* **2010**, *49*, 7281−7283.

(17) Chen, C.; Geng, J.; Pu, F.; Yang, X.; Ren, J.; Qu, X. Polyvalent Nucleic Acid/Mesoporous Silica Nanoparticle Conjugates: Dual Stimuli-Responsive Vehicles for Intracellular Drug Delivery. *Angew. Chem., Int. Ed.* **2011**, *50*, 882−886.

(18) Chen, C.; Pu, F.; Huang, Z.; Liu, Z.; Ren, J.; Qu, X. Stimuli-Responsive Controlled-Release System Using Quadruplex DNA-Capped Silica Nanocontainers. *Nucleic Acids Res.* **2011**, *39*, 1638−1644.

(19) Yuan, Q.; Zhang, Y.; Chen, T.; Lu, D.; Zhao, Z.; Zhang, X.; Li, Z.; Yan, C.-H.; Tan, W. Photon-Manipulated Drug Release from a Mesoporous Nanocontainer Controlled by Azobenzene-Modified Nucleic Acid. *ACS Nano* **2012**, *6*, 6337−6344.

(20) He, D.; He, X.; Wang, K.; Cao, J.; Zhao, Y. A Photon-Fueled Gate-Like Delivery System Using i-Motif DNA Functionalized Mesoporous Silica Nanoparticles. *Adv. Funct. Mater.* **2012**, *22*, 4704−4710.

(21) Zhou, S.; Du, X.; Cui, F.; Zhang, X. Multi-Responsive and Logic Controlled Release of DNA-Gated Mesoporous Silica Vehicles Functionalized with Intercalators for Multiple Delivery. *Small* **2014**, *10*, 980−988.

(22) Luo, Z.; Cai, K.; Hu, Y.; Zhao, L.; Liu, P.; Duan, L.; Yang, W. Mesoporous Silica Nanoparticles End-Capped with Collagen: Redox-Responsive Nanoreservoirs for Targeted Drug Delivery. *Angew. Chem., Int. Ed.* **2011**, *50*, 640−643.

(23) Schlossbauer, A.; Kecht, J.; Bein, T. Biotin-Avidin as a Protease-Responsive Cap System for Controlled Guest Release from Colloidal Mesoporous Silica. *Angew. Chem., Int. Ed.* **2009**, *48*, 3092−3095.

(24) Climent, E.; Bernardos, A.; Martínez-Máñez, R.; Maquieira, A.; Marcos, M. D.; Pastor-Navarro, N.; Puchades, R.; Sancenón, F.; Soto, J.; Amorós, P. Controlled Delivery Systems Using Antibody-Capped Mesoporous Nanocontainers. *J. Am. Chem. Soc.* **2009**, *131*, 14075−14080.

(25) Smith, E. A.; Thomas, W. D.; Kiessling, L. L.; Corn, R. M. Surface Plasmon Resonance Imaging Studies of Protein-Carbohydrate Interactions. *J. Am. Chem. Soc.* **2003**, *125*, 6140−6148.

(26) Liang, P.-H.; Wang, S.-K.; Wong, C.-H. Quantitative Analysis of Carbohydrate-Protein Interactions Using Glycan Microarrays: Determination of Surface and Solution Dissociation Constants. *J. Am. Chem. Soc.* **2007**, *129*, 11177−11184.

(27) Zheng, H.; Du, X. Enhanced Binding and Biosensing of Carbohydrate-Functionalized Monolayers to Target Proteins by Surface Molecular Imprinting. *J. Phys. Chem. B* **2009**, *113*, 11330−11337.

(28) Zheng, H.; Du, X. Reduced Steric Hindrance and Optimized Spatial Arrangement of Carbohydrate Ligands in Imprinted Monolayers for Enhanced Protein Binding. *Biochim. Biophys. Acta* **2013**, *1828*, 792−800.

(29) Wu, S.; Huang, X.; Du, X. Glucose- and pH-Responsive Controlled Release of Cargo from Protein-Gated Carbohydrate-Functionalized Mesoporous Silica Nanocontainers. *Angew. Chem., Int. Ed.* **2013**, *52*, 5580−5584.

(30) Maloney, K. M.; Schief, W. R., Jr.; Pack, D. W.; Frey, W.; Arnold, F. H.; Vogel, V. Binding and Two-Dimensional Crystallization of Streptavidin at the Air/Water Interface via Engineered Cu-IDA Chelator Lipids. *Coord. Chem. Rev.* **1999**, *183*, 3−18.

(31) Kent, M. S.; Yim, H.; Sasaki, D. Y.; Satija, S.; Majewski, J.; Gog, T. Analysis of Myoglobin Adsorption to Cu(II)-IDA and Ni(II)-IDA Functionalized Langmuir Monolayers by Grazing Incidence Neutron and X-Ray Techniques. *Langmuir* **2004**, *20*, 2819−2829.

(32) Kent, M. S.; Yim, H.; Sasaki, D. Y.; Satija, S.; Seo, Y.-S.; Majewski, J. Adsorption of myoglobin to Cu(II)-IDA and Ni(II)-IDA Functionalized Langmuir Monolayers: Study of the Protein Layer Structure during the Adsorption Process by Neutron and X-Ray Reflectivity. *Langmuir* **2005**, *21*, 6815−6824.

(33) Haddour, N.; Cosnier, S.; Gondran, C. Electrogeneration of a Poly(pyrrole)-NTA Chelator Film for a Reversible Oriented Immobilization of Histidine-Tagged Proteins. *J. Am. Chem. Soc.* **2005**, *125*, 5752−5753.
(34) Johnson, D. L.; Martin, L. L. Controlling Protein Orientation at Interfaces Using Histidine Tags: An Alternative to Ni/NTA. *J. Am. Chem. Soc.* **2005**, *127*, 2018−2019.
(35) Wegner, S. V.; Spatz, J. P. Cobalt(III) as a Stable and Inert Mediator Ion between NTA and His6-Tagged Proteins. *Angew. Chem., Int. Ed.* **2013**, *52*, 7593−7596.
(36) Todd, R. J.; Johnson, R. D.; Arnold, F. H. Multiple-Site Binding Interactions in Metal-Affinity Chromatography: 1. Equilibrium Binding of Engineered Histidine-Containing Cytochromes *c*. *J. Chromatogr., A* **1994**, *662*, 13−26.
(37) Yang, X.; Li, Z.; Li, M.; Ren, J.; Qu, X. Fluorescent Protein Capped Mesoporous Nanoparticles for Intracellular Drug Delivery and Imaging. *Chem.−Eur. J.* **2013**, *19*, 15378−15383.
(38) Yim, H.; Kent, M. S.; Sasaki, D. Y.; Polizzotti, B. D.; Kiick, K. L.; Majewski, J.; Satija, S. Rearrangement of Lipid Ordered Phases upon Protein Adsorption due to Multiple Site Binding. *Phys. Rev. Lett.* **2006**, *96*, 198101.
(39) Tarn, D.; Xue, M.; Zink, J. I. pH-Responsive Dual Cargo Delivery from Mesoporous Silica Nanoparticles with a Metal-Latched Nanogate. *Inorg. Chem.* **2013**, *52*, 2044−2049.